JACS
JOURNAL OF THE AMERICAN CHEMICAL SOCIETY
Article
pubs.acs.org/JACS

Polyoxometalate-Catalyzed Insertion of Oxygen from O_2 into Tin−Alkyl Bonds

Alexander M. Khenkin, Irena Efremenko, Jan M. L. Martin, and Ronny Neumann*

Department of Organic Chemistry, Weizmann Institute of Science, Rehovot, Israel 76100

Supporting Information

ABSTRACT: The polyoxometalate $H_5PV_2Mo_{10}O_{40}$ mediates the insertion of an oxygen atom from $H_5PV_2Mo_{10}O_{40}$ into the tin−carbon bond of *n*-Bu_4Sn through its activation by electron transfer to yield 1-butanol and $(n\text{-}Bu_3Sn)_2O$. The reaction is initiated by electron transfer from *n*-Bu_4Sn to $H_5PV^{V}_{2}Mo_{10}O_{40}$ to yield the ion pair $n\text{-}Bu_4Sn^{\bullet+}-H_5PV^{IV}V^{V}Mo_{10}O_{40}$. The $H_5PV^{IV}V^{V}Mo_{10}O_{40}$ moiety was identified by UV−vis and EPR. DFT calculations show that $n\text{-}Bu_4Sn^{\bullet+}-H_5PV^{IV}V^{V}Mo_{10}O_{40}$ is relatively unstable and forms more stable Bu^+ and Bu_3Sn^+ cations coordinated to the polyoxometalate, which were also identified by ESI-MS. Products are released at higher temperatures. In the presence of molecular oxygen as the terminal oxidant the reaction is catalytic.

INTRODUCTION

The selective oxygenation of hydrocarbons, especially using ground-state O_2 as the oxygen donor, remains an important and significant research challenge. The ubiquitous reaction of O_2 with hydrocarbons occurs by autoxidation pathways with free radical intermediates that often preclude the selective formation of mono-oxygenated products.[1] As pertains to the selective oxygenation of alkanes, for example hydroxylation, both C−H bond activation and C−O bond formation at a transition-metal center are required. Enzymes such as methane monooxygenase, cytochrome P450, and others typically form high-valent and highly reactive iron− or copper−oxo intermediates from O_2 *under reducing conditions* that lead to insertion of oxygen into C−H bonds.[2] An alternative strategy was suggested quite long ago by Shilov and co-workers, where a C−H bond activation, e.g. of methane, takes place at a Pt^{II} catalytic site and reported nucleophilic attack of water after formation of a Pt^{IV} intermediate leads to oxygenation.[3] There are, however, only a few examples where this reaction was carried out with O_2 to form the Pt^{IV} intermediate.[4] Recently, Gunnoe, Groves, and co-workers have outlined a pathway where an insertion of an oxygen atom into a M−C bond leads to formation of an alkoxide complex that then can activate a C−H bond for 1,2-addition across the M−OR bond to form a metal hydrocarbyl complex and a free alcohol.[5] There are only a few examples of oxygen insertion into M−C bonds,[6] and it would appear that the Baeyer−Villiger type oxidation of methylrhenium trioxide via formation of η^2-peroxo species is the most studied reaction.[7] Recently, a flavin-catalyzed version of this reaction was reported with H_2O_2 as the oxidant.[5]

We have shown that phosphovanadomolybdates, notably the $H_5PV_2Mo_{10}O_{40}$ polyoxometalate of the α-Keggin structure, can insert oxygen into C−H bonds of arenes and alkylarenes[8] and primary and vicinal alcohols[9] by an electron transfer−oxygen transfer type mechanism.[10] Advantageously, such reactions can be catalytic with *molecular oxygen* as terminal oxidant. Now we report that $H_5PV_2Mo_{10}O_{40}$ can insert oxygen atoms into the Sn−C bond of tin−alkyl compounds such as *n*-Bu_4Sn and that this reaction can be catalytic with O_2 as terminal oxidant to yield primary alcohols (Scheme 1).

Scheme 1. Aerobic Oxygenation of Tetrabutyltin Catalyzed by $H_5PV_2Mo_{10}O_{40}$

$$2\ (n\text{-Bu})_4\text{Sn} + O_2 + H_2O \xrightarrow{H_5PV_2Mo_{10}O_{40}} [(n\text{-Bu})_3\text{Sn}]_2O + 2\ 1\text{-BuOH}$$

RESULTS AND DISCUSSION

Anaerobic Reactions. The oxygenation of *n*-Bu_4Sn by oxygen transfer from $H_5PV_2Mo_{10}O_{40}$ was first studied under *anaerobic* reaction conditions. Thus, 0.029 mmol *n*-Bu_4Sn and 0.01 mmol of $H_5PV_2Mo_{10}O_{40}$ in 1 mL of acetonitrile reacted at 70 °C under Ar for 2 h to quantitatively yield 1-BuOH (~0.005 mmol), a mixture of 1-butene, 2-butene, and 2-methylpropene (~0.005 mmol, 1:1:1 ratio), and ~0.005 mmol of $(n\text{-}Bu_3Sn)_2O$, as analyzed by GC-FID and GC-MS. The result that on the one hand only the primary alcohol was formed while all isomeric butene compounds were formed is notable, as is the anaerobic reaction stoichiometry that shows that each equivalent of $H_5PV_2Mo_{10}O_{40}$ yielded a combined 1 equiv of 1-butanol and isomeric butenes. Other solvents gave different 1-butanol/butene ratios, while some solvents were not suitable (Table S1, Supporting Information). The acid form of the polyoxometalate was required or a relatively strong acid such as trifluoroacetic acid needed to be added to the reaction (Figure S1, Supporting Information).

Received: September 29, 2013
Published: December 6, 2013

dx.doi.org/10.1021/ja409559h | J. Am. Chem. Soc. 2013, 135, 19304−19310

$H_4PVMo_{11}O_{40}$ was equally reactive, and $H_3PMo_{12}O_{40}$ showed less reactivity that was increased by ~55% in the presence of $VO(O\text{-}i\text{-}Pr)_3$, likely due to the in situ formation of a phosphovanadomolybdate. Analogous tungstates were not reactive, nor was a monomeric vanadate such as $VO(O\text{-}i\text{-}Pr)_3$ or a decavanadate with or without added acid. These latter compounds have never been observed to be active in electron transfer–oxygen transfer type reactions.[10]

During the anaerobic reaction $H_5PV_2Mo_{10}O_{40}$ was reduced, as evidenced by the formation of a heteropoly blue compound (λ_{max} 750 nm).[11] Furthermore, very similar to what was reported in the past,[12] the typical EPR spectrum for the V(IV) containing polyoxometalate (Figure 1) shows the presence of

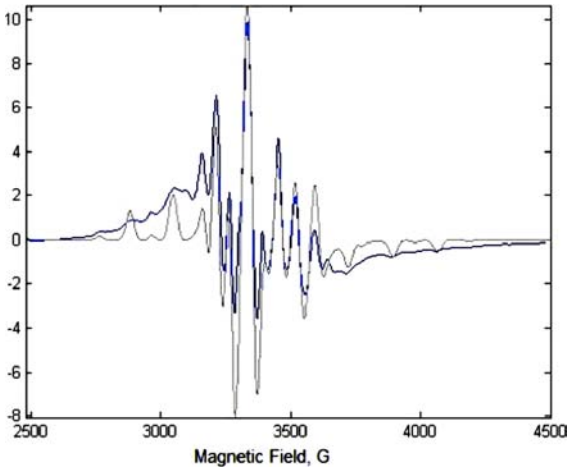

Figure 1. EPR spectrum resulting from the reaction of n-Bu_4Sn and $H_5PV_2Mo_{10}O_{40}$: (black) experimental; (gray) simulation. The spectrum was obtained by heating 29 mM n-Bu_4Sn and 1.5 mM $H_5PV_2Mo_{10}O_{40}$ in acetonitrile under argon at 50 °C for 20 min in a quartz capillary tube (3 mm, 100 μL). Spectra were recorded at 100 K: microwave frequency, 9.424 GHz; microwave power, 12 mW; field modulation, 1 G; receiver gain, 60; time constant, 1310 ms; scan time, 200 s. The simulation reveals that the spectrum contains two type of vanadium atoms in a ~65/35 ratio. Species 1 (65%): $g_\perp$= 1.980, $g_\parallel$ = 1.937, $A_\perp$ = 165 G, $A_\parallel$ = 459 G. Species 2 (35%): $g_\perp$ = 1.977, $g_\parallel$ = 1.936, $A_\perp$ = 150 G, $A_\parallel$ = 550 G.

two species related to reduced $H_5PV_2Mo_{10}O_{40}$: one where VO^{2+} is supported on the polyoxometalate (major species, ~65%) and one where the vanadium is incorporated within the polyoxometalate (minor species, ~35%). Together the UV–vis and EPR spectra indicate an electron transfer oxidation of n-Bu_4Sn.

The importance of the initiation of the reaction by electron transfer from the alkyltin substrate to $H_5PV_2Mo_{10}O_{40}$ is also observable by comparing the reactivity of n-Bu_4Sn to that of Me_4Sn (0.2 mmol of substrate, 0.1 mmol of $H_5PV_2Mo_{10}O_{40}$, 10 mL of acetonitrile, 70 °C, Ar, 2 h). Analysis was by GC-FID and GC-MS. Under identical conditions n-Bu_4Sn (ionization potential 8.76 eV)[13] reacted 25 times faster, yielding 100 μmol (~100% yield) of products, than Me_4Sn (ionization potential 9.69 eV),[13] which yielded only 8 μmol (8% yield) of MeOH. It should be noted that these literature values represent vertical gas phase ionization potentials. Our DFT calculations (vide infra) yielded a *vertical* ionization potential for n-Bu_4Sn of 8.48 eV, in good agreement with experiment. The calculated *adiabatic* ionization potentials for n-Bu_4Sn and Me_4Sn are 7.8 and 9.1 eV in the gas phase and 5.7 and 6.7 eV in acetonitrile, respectively.

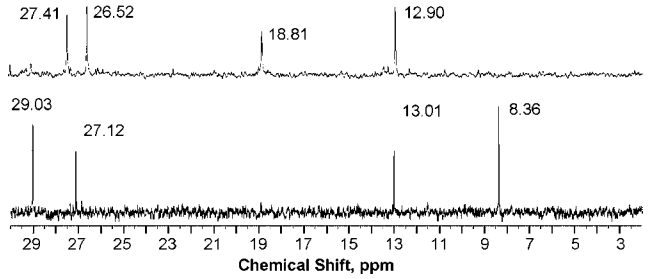

Figure 2. ^{13}C NMR spectra of $(n\text{-}Bu)_4Sn$ in CD_3CN (bottom) and of a 1/1 $(n\text{-}Bu)_4Sn/H_5PV_2Mo_{10}O_{40}$ mixture after 2 h at 70 °C.

The reaction between $H_5PV_2Mo_{10}O_{40}$ and n-Bu_4Sn was further studied by ^{13}C and ^1H NMR. In Figure 2 (bottom), the spectrum of n-Bu_4Sn shows peaks at 29.0, 27.1, 13.0, and 8.4 ppm assigned to the β, γ, δ, and α carbon atoms, respectively. After n-Bu_4Sn was heated for 2 h at 70 °C under Ar in the presence of 1 equiv of $H_5PV_2Mo_{10}O_{40}$ (Figure 2, top), a new spectrum was measured with four peaks at 27.4, 26.5, 18.7, and 12.9 ppm attributable to an intermediate species that is only slightly different than the spectrum of $(n\text{-}Bu_3Sn)_2O$. Notably no 1-butanol, butene isomers, or $(n\text{-}Bu_3Sn)_2O$ was observed in the NMR spectra.[14] A similar ^1H NMR experiment (Figure S2, Supporting Information) also revealed such an intermediate, which by integration indicated formation of 1 equiv of intermediate per 2 equiv of n-Bu_4Sn using 1,2-dichloroethane as internal standard. The ^{119}Sn and ^{51}V NMR spectra were very broadened and featureless, apparently due to the presence of paramagnetic vanadium(IV) and possibly spin on the tin atom. The ^{31}P NMR spectrum showed the residual presence (very low intensity) of some nonreduced polyoxometalate.

Clearly, the final reaction products, 1-butanol and butenes, previously observed as noted above were released upon injection into the GC due to the elevated temperature, 220 °C, at the injection port. The final products including $(n\text{-}Bu_3Sn)_2O$ can, however, be isolated by using the following procedure. n-Bu_4Sn (10 μmol) and $H_5PV_2Mo_{10}O_{40}$ (10 μmol) in 10 mL of acetonitrile were reacted under Ar to produce a blue solution. The acetonitrile was evaporated off, and the solid residue was heated at 120 °C for 1 h in a pressure tube. After cooling, a GC-MS and GC analysis of the gas phase was carried out and the three isomeric butenes (1-butene, 2-butene, and isobutene in the ratio 1/1/1) were found. Then 1-butanol and $(n\text{-}Bu_3Sn)_2O$ were extracted from the solid slurry by $CDCl_3$. This solution shows ^{13}C NMR and ^1H NMR spectra characteristic of 1-butanol and $(n\text{-}Bu_3Sn)_2O$ in $CDCl_3$.[14] The amount of 1-butanol determined from this solution and was approximately 5 μmol. The ratio, determined by ^1H NMR, of 1-butanol to $(n\text{-}Bu_3Sn)_2O$ is 1/0.9, which is only slightly different than the theoretical ratio, which should be 1/1 assuming equal amounts of 1-butanol and butene isomers are formed. This experiment confirms the reaction stoichiometry shown in Scheme 2, where the oxidant, [O], is $H_5PV_2Mo_{10}O_{40}$, as will be elaborated upon below.

Further information on possible intermediates was obtained by electrospray ionization mass spectrometry (ESI-MS; Figure 3).[15] Although the negative ion spectrum is dominated by peaks at $m/z \leq 882$ attributable to the fragmentation of $H_5PVMo_{11}O_{40}$, peaks at $m/z \geq 1056$ can be assigned to the fragmentation of $(n\text{-}Bu_4Sn)_x\text{-}H_4PVMo_{11}O_{40}$ (x = 1, 2) intermediates, as summarized in Scheme 3. Importantly, in the positive ion mode, in addition to the typical peaks associated with the fragmentation of n-Bu_4Sn, we were able to identify a fragment centered at m/z

dx.doi.org/10.1021/ja409559h | J. Am. Chem. Soc. 2013, 135, 19304–19310

Scheme 2. Stoichiometry of the Reaction between $(n\text{-Bu})_4Sn$ and $H_5PV_2Mo_{10}O_{40}$

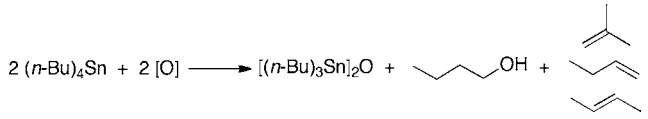

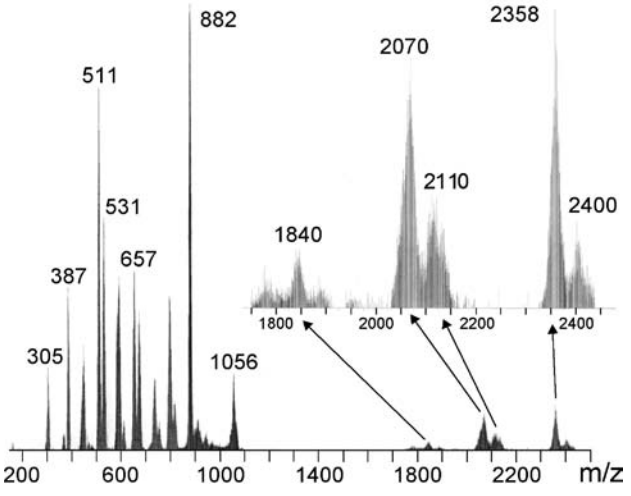

Figure 3. Negative ion ESI-MS of a 1/1 $(n\text{-Bu})_4Sn/H_4PVMo_{11}O_{40}$ mixture.

Scheme 3. Assignment of the ESI-MS Spectrum

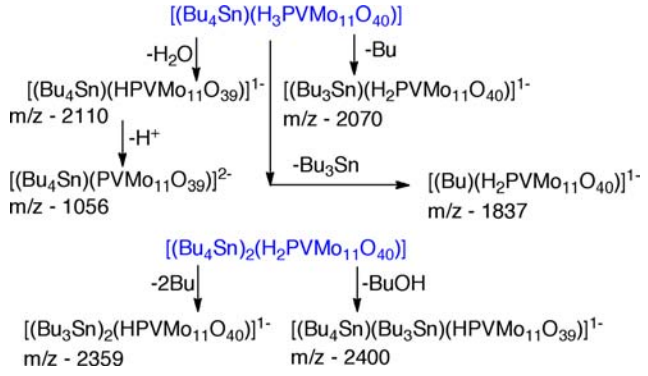

665.17 with an isotope distribution fitting for a $[(Bu_3Sn)_2OVOH_2]^+$ species. This is an indication of binding of the incipient reaction product, $(n\text{-Bu}_3Sn)_2O$ (Scheme 1), to the polyoxometalate. Notably, also a butyl-polyoxometalate fragment was observed (Scheme 3).

The kinetics of the reaction of $H_5PV_2Mo_{10}O_{40}$ with $n\text{-Bu}_4Sn$ was studied by following the reduction of $H_5PV_2Mo_{10}O_{40}$ by UV−vis spectroscopy. Thus, 15 mM $n\text{-Bu}_4Sn$ and 0.25−2 mM $H_5PV_2Mo_{10}O_{40}$ in acetonitrile were reacted at 50 °C. A log k_{obs} versus log $[H_5PV_2Mo_{10}O_{40}]$ plot (Figure S3, Supporting Information) shows that the reaction is first order (slope 1.02) in $H_5PV_2Mo_{10}O_{40}$. Similarly, changing the concentration of $n\text{-Bu}_4Sn$ (1.7−29 mM) at a constant concentration of $H_5PV_2Mo_{10}O_{40}$ (1 mM) shows that the reaction is first order in $n\text{-Bu}_4Sn$ (slope 1.003). Therefore, the reactions are second order overall (eq 1), with a second-order rate constant of

$$d[H_5PV_2Mo_{10}O_{40}(red)]/dt = k[H_5PV_2Mo_{10}O_{40}][Bu_4Sn] \quad (1)$$

1.5×10^{-2} M^{-1} s^{-1}, which is the same order of magnitude found for the oxidation of $n\text{-Bu}_4Sn$ to a cation radical by hexachloroiridate(IV) that has a redox potential similar to that of $H_5PV_2Mo_{10}O_{40}$.[13] Eyring plots of the rate constants as a function of temperature (Figure S4, Supporting Information) yielded the following values for the activation energy, enthalpy, entropy, and free energy of activation: ΔE_a = 14.6 kcal/mol, $\Delta H^{\ddagger}_{323}$ = 14.0 kcal/mol, $\Delta S^{\ddagger}_{323}$ = −29.6 eu, $\Delta G^{\ddagger}_{323}$ = 23.6 kcal/mol.

Oxygen insertion into the Sn−C bond was studied by reacting 10 mM $H_5PV_2Mo_{10}{}^{18}O_{40}$ (40−50% ^{18}O) with 29 mM $n\text{-Bu}_4Sn$ in CH_3CN at 70 °C under Ar. The reaction yielded 1-butanol (43%^{18}O) and $(n\text{-Bu}_3Sn)_2O$ (45% ^{18}O), as determined by mass spectrometry. Clearly, there is *quantitative* oxygen transfer from the polyoxometalate to both oxygenated products.

Aerobic Reactions. Catalytic aerobic oxidation ($n\text{-Bu}_4Sn$ (2.9 mmol) and $H_5PV_2Mo_{10}O_{40}$ (0.10 mmol) in 10 mL of CH_3CN, 70 °C, 1 bar of O_2, 7 h) yielded both 1-butanol and butenes in a ∼9/1 molar ratio (1.2 mmol, 12 turnovers) as well as ∼0.6 mmol of $(n\text{-Bu}_3Sn)_2O$. The same reaction using $^{18}O_2$ (95% ^{18}O) yielded 1-BuOH (84% ^{18}O) and $(n\text{-Bu}_3Sn)_2O$ (16% ^{18}O). Therefore, under aerobic conditions, the oxygen atom in 1-butanol comes mostly from O_2, whereas the oxygen atom in $(n\text{-Bu}_3Sn)_2O$ is mostly from the polyoxometalate. Some labeling of the latter occurs, possibly because under turnover conditions defect oxygen structures of the polyoxometalate after oxygen transfer are "replenished" by $^{18}O_2$. Support for this scenario comes also by carrying out a reaction in the presence of S_8. Thus, $n\text{-Bu}_4Sn$ (2.9 mmol), $H_5PV_2Mo_{10}O_{40}$ (0.10 mmol), and S_8 (4.0 mmol) in 10 mL of CH_3CN at 70 °C under argon were reacted for 7 h and then analyzed by GC-FID and GC-MS. Di- and trisulfides, $(n\text{-Bu}_3)_2S_x$ (x = 2, 3), were formed and also $(n\text{-Bu}_3Sn)_2O$ was obtained but $(n\text{-Bu}_3Sn)_2S$ was not.

Calculations on the Anaerobic Reaction. Mechanistic insight into the oxidation of $n\text{-Bu}_4Sn$ with $H_5PV_2Mo_{10}O_{40}$ using the 1,2-isomer as an exemplary polyoxometalate was obtained using density functional theory (DFT) calculations.[16] Thermodynamic considerations show that the overall oxygen transfer reaction according to eq 2 is exergonic by 16.6−18.8 kcal/mol depending on the butene isomer formed at 70 °C in acetonitrile.

$$2n\text{-Bu}_4Sn + 2H_5PV^{V}{}_2Mo_{10}O_{40} \rightarrow O(n\text{-Bu}_3Sn)_2 + BuOH + C_4H_8 + 2H_5PV^{IV}{}_2Mo_{10}O_{39} \quad (2)$$

However, since $H_5PV_2Mo_{10}O_{40}$ is hydrated with ∼35 molecules of water, explicit consideration of a water molecule in close proximity to the reaction site of $H_5PV_2Mo_{10}O_{40}$ shows that it will readily occupy the oxygen defect site of the deoxygenated compound, $H_5PV_2Mo_{10}O_{39}$, with an energy gain of 14.4 kcal/mol, thus rendering the oxygenation reaction even more exergonic (eq 3). ΔG_{343} ranges from −45.4 to −47.6 kcal/mol depending on the butene isomers formed.

$$H_5PV^{IV}{}_2Mo_{10}O_{39} + H_2O \rightarrow H_7PV^{IV}{}_2Mo_{10}O_{40} \quad (3)$$

As previously shown, oxidation reactions with $H_5PV_2Mo_{10}O_{40}$ are inclined to outer-sphere reactions of proton transfer (PT), electron transfer (ET), and coupled proton and electron transfer (CPET) as the first step in the reaction pathway.[17] In this case the calculations demonstrate that ET is exergonic in a polar solution while other outer-sphere reactions are endergonic (Scheme 4).[18]

dx.doi.org/10.1021/ja409559h | J. Am. Chem. Soc. 2013, 135, 19304−19310

Scheme 4. Calculated ΔG_{343} in kcal/mol for Outer-Sphere Interactions of $H_5PV_2^{V}Mo_{10}O_{40}$ with *n*-Bu_4Sn in Acetonitrile

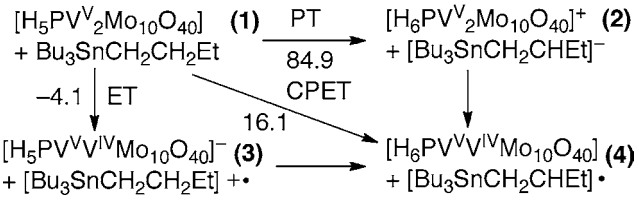

The ESI-MS data showing species where *n*-Bu_4Sn is coordinated to the polyoxometalate prompted a more detailed investigation of the ET process. Indeed, we found that formation of complex **5** (Figure 4), in which the tin atom is bound, with a

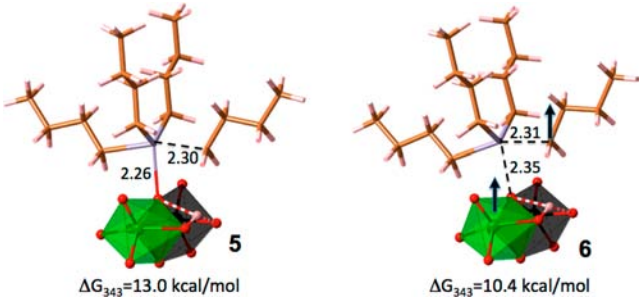

Figure 4. Optimized geometry of *n*-Bu_4Sn coordinated to the bridging oxygen atom of $H_5PV_2Mo_{10}O_{40}$ before (complex **5**) and after ET (complex **6**).

bond energy of 8 kcal/mol, to a bridging oxygen atom of the polyoxometalate (Figure 4), precedes ET. In this complex there is a strong distortion of the coordination sphere around the tin atom with an increase of ∠C−Sn−C from 109.7° in *n*-Bu_4Sn to 166.8° in **5**. This deformation makes complex **5** less energetically favorable by 13.0 kcal/mol and determines the activation barrier for reduction of the polyoxometalate.[19] Such a deformation is more favorable for *n*-Bu_4Sn in the triplet state than in the singlet state. Thus, the subsequent formation of the triplet complex **6** (Figure 4) proceeds with an energy gain of 2.6 kcal/mol and results in the ET from *n*-Bu_4Sn to $H_5PV_2Mo_{10}O_{40}$. The highest occupied orbital in *n*-Bu_4Sn is mostly localized along the Sn−C bond (Figure S5, Supporting Information); thus, both coordination to the strongly electronegative O atom in **5** and the ET in **6** lead to a considerable lengthening of one Sn−C bond, from 2.20 Å in *n*-Bu_4Sn to 2.30 Å in **5** and 2.31 Å in **6**. Moreover, the ET causes significant elongation of the O−Sn bond, from 2.26 Å in **5** to 2.35 Å in **6**. The bonding pattern in **6** allows for three further possible transformations, as detailed below.

(i) The energetically most favorable transformation of **6** (Scheme 5(i)) involves the breaking of a Sn−C bond with formation of $[SnBu_3^{+}$-$H_5PV^{IV}V^{V}Mo_{10}O_{40})]$ (complex **7**) and the formation of a butyl radical, Bu• (Figure 5). The latter is quickly trapped by another molecule of $H_5PV_2Mo_{10}O_{40}$ to form $[Bu^{+}$-$(H_5PV^{IV}V^{V}Mo_{10}O_{40})]$ (complex **8**) (Figure 5).

(ii) Cleavage of the Sn−O bond yielding $[H_5PV^{IV}V^{V}Mo_{10}O_{40}]^{-}$ (complex **3**) and $SnBu_4^{\bullet+}$ is energetically less favorable (Scheme 5(ii)). One of the Sn−C bonds in $SnBu_4^{\bullet+}$ is further lengthened from 2.31 Å in **6** to 2.48 Å in $SnBu_4^{\bullet+}$, with a corresponding change in the Wiberg bond index (WBI) from 0.67 to 0.26.[20] The subsequent cleavage of the Sn−C bond to yield Bu• and $(n\text{-Bu})_3Sn^{+}$

Scheme 5. Scenarios for the Transformation of Complex 6

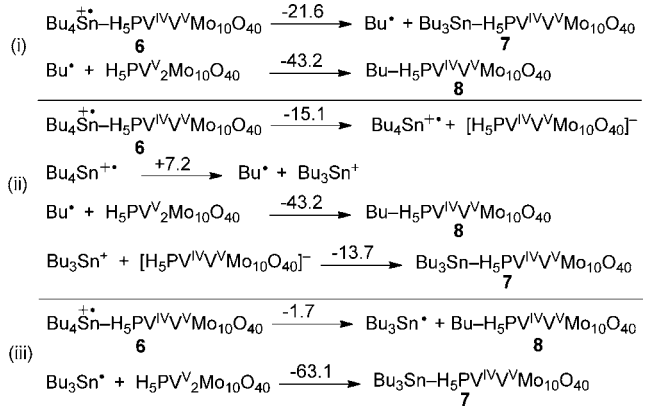

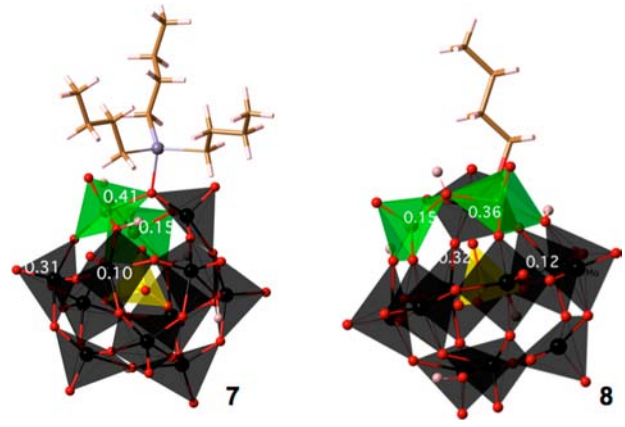

Figure 5. Geometry and localization of the highest spin density in complexes **7** and **8**.

is slightly uphill, but this is compensated by their interaction with the polyoxometalate to yield complexes **7** and **8**.

(iii) The least favorable transformation involves cleavage of a Sn−C bond (Scheme 5(iii)) with formation of **8** (Figure 5) and release of $SnBu_3^{\bullet}$, which in turn is stabilized by reaction with $H_5PV_2Mo_{10}O_{40}$.

Thus, all three transformations of complex **6** lead to the same reaction products **7** and **8** with a total energy gain of 64.8 kcal/mol. The Bu^{+} cation in **8** is strongly bound to bridging oxygen atoms (WBI = 0.84), while the $SnBu_3^{+}$ cation in **7** is only weakly bonded to the bridging oxygen atom (WBI = 0.25). The spin density in these complexes is mainly localized on the V and Mo atoms adjacent to the coordination sites (Figure 5). It is therefore reasonable that **7** and **8** are not observable by ^{13}C and ^{1}H NMR.

The release of 1-butanol from **8** requires the cleavage of adjacent V−O and Mo−O bonds. Although these bonds are weakened, this reaction was found to be thermodynamically unfavorable and kinetically forbidden at 70 °C in acetonitrile. The lowest energy pathways for the transformation of an ion-pair complex involves traces of water that facilitate the formation of defect structures with coordinatively unsaturated sites (CUS).[17] In this way **9** (Figure 6) is formed from **8**, where the 1-butanol fragment is weakly bound to the vanadium atom of the defect site (WBI = 0.32). Release of 1-butanol with subsequent closing of the defect site (Figure 6) results in formation of $H_7PV^{IV}_2Mo_{10}O_{40}$, where a bridging oxygen atom has been replaced by an oxygen atom from water. This mechanistic

dx.doi.org/10.1021/ja409559h | J. Am. Chem. Soc. 2013, 135, 19304−19310

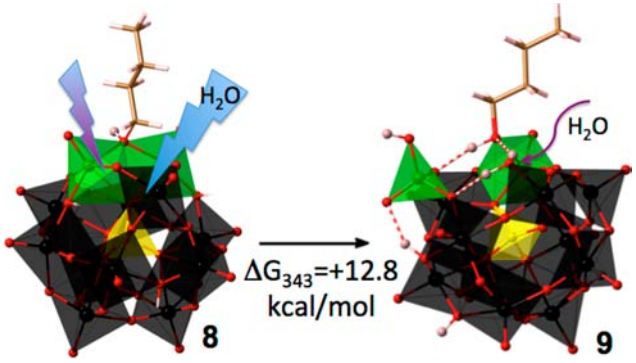

Figure 6. Water-assisted formation of the defect complex **9** showing that the O atom in the weakly bound 1-butanol fragment originates from the polyoxometalate lattice while the water molecule saturates the CUS.

scenario is in agreement with the observed formation of 1-butanol as the only alcohol product and with the oxygen atom in 1-butanol originating from the polyoxometalate lattice. The coordinated butyl can undergo dehydrogenation with formation of *n*-butene. This reaction is more favorable than oxygenation by 3.6 kcal/mol at 70 °C in acetonitrile.

In the similar defect structure 7-H_2O formed in the presence of an inner-sphere water molecule, a coordinated $(n\text{-Bu})_3$SnOH moiety remains strongly bonded to the V atom of the defect site (WBI = 0.45) and its subsequent dissociation is not a feasible step toward the oxygenated product. On the other hand, extremely high negative charge on the oxygen atom bound to $SnBu_3^+$ favors bonding of $(n\text{-Bu})_3Sn^\bullet$ (Scheme 5(iii)) to yield coordinated $(n\text{-Bu}_3Sn)_2O$.[21] This bulky moiety is especially stable in the presence of two inner-sphere water molecules that mediate the very open defect complex **10** (Figure 7), in which a V atom bound to $(n\text{-Bu}_3Sn)_2O$ is connected to the remainder of the polyoxometalate structure by only one bond: i.e., it closely resembles the $[(Bu_3Sn)_2\text{-}OVOH_2]^+$ species observed by ESI-MS. Moreover, the distance between the displaced V atom and the central P in this complex is 5.55 Å, much longer than the typical V−P distance in the POM (~3.55 Å). This complex is the major V(IV)-containing species observed in the EPR spectrum (Figure 1), as also discussed previously for other oxidation reactions.[12,16a] The calculations show that **10** has a closed-shell electronic configuration in the ground state, whereas the lowest energy diradical form is 5.8 kcal/mol higher in energy. Complex **10** seems to be the only stable product in the reaction mixture that is likely to be observable by ^{13}C and ^1H NMR, as found experimentally. Release of $(n\text{-Bu}_3Sn)_2O$ at higher temperature would result in an ^{18}O-labeled product, as observed, and formation of $H_7PV^{IV}{}_2Mo_{10}O_{40}$, where a bridging oxygen atom has been replaced by an oxygen atom from water.

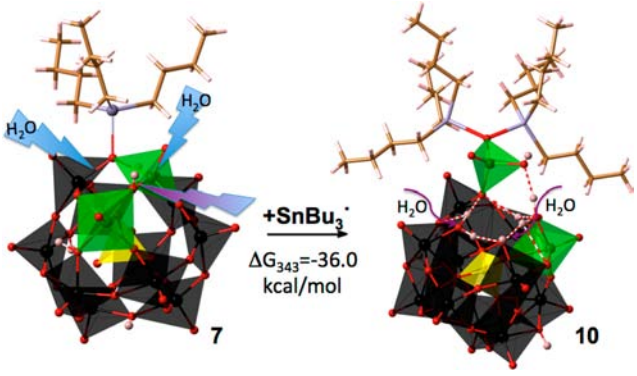

Figure 7. Water-assisted formation of defect complex **10**.

CONCLUSIONS

The reaction of phosphomolybdates, $H_{3+x}PV_xMo_{12-x}O_{40}$, where x = 1, 2, with n-Bu_4Sn under anaerobic reaction conditions proceeds by electron transfer from n-Bu_4Sn to the polyoxometalate, as observed experimentally by UV−vis and EPR spectrometry. At 70 °C under argon the oxygenated or dehydrogenated products are not released *but* the formation of the incipient products can be observed by ESI-MS. Thus, there is inner-sphere formation of the coordinated oxygenated products after the initial electron transfer. At higher temperatures of 120 °C and above the products are released with the expected reaction stoichiometry, as delineated in Scheme 2. We have used DFT to gain a mechanistic understanding; Figure 8 summarizes the energy profile obtained from the calculations.[22] The computations show that an initial interaction between n-Bu_4Sn and $H_5PV_2Mo_{10}O_{40}$ leads to the ion pair n-$Bu_4Sn^{\bullet+}$−$H_5V^{IV}V^VMo_{10}O_{40}$ (**6**). At this point three exergonic scenarios were identified, through cleavage of Sn−C or Sn−O bonds yielding butyl and tributyltin radicals or cations that react with the polyoxometalate leading to two paramagnetic intermediates, Bu^+−$H_5V^{IV}V^VMo_{10}O_{40}$ (**7**) and n-Bu_3Sn^+−$H_5V^{IV}V^VMo_{10}O_{40}$ (**8**).[23] Likely these open-shell intermediates cannot be observed by NMR. Bu^+−$H_5V^{IV}V^VMo_{10}O_{40}$ yields 1-butanol and butenes at higher temperatures, but n-Bu_3Sn−$H_5V^{IV}V^VMo_{10}O_{40}$ apparently reacts with a tributyltin radical to yield a closed-shell intermediate, $(n\text{-Bu}_3Sn)O$− $H_5V^{IV}V^VMo_{10}O_{39}$, with a defect structure that was identified by ESI-MS and NMR. Release of 1-BuOH, butenes, and $(n\text{-Bu}_3Sn)O$ is possible at higher temperatures in the presence of water through coordinatively unsaturated species in a reaction that is in part thermodynamically driven by the formation of the two-electron-reduced $H_7PV^{IV}{}_2Mo_{10}O_{40}$.[24] The isomerization of *n*-butene is known to be polyoxometalate acid catalyzed at >100 °C.[25]

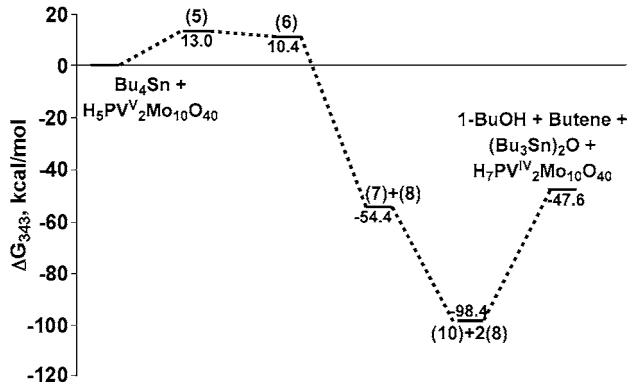

Figure 8. Relative energies of the key intermediates in the anaerobic oxidation of n-Bu_4Sn at 70 °C in acetonitrile.

Despite the fact that products are not released under anaerobic reaction conditions at 70 °C, under O_2 the reactions *do proceed catalytically* with formation of products. Here $H_4PVMo_{11}O_{40}$ was found to be less effective. Experiments indicate that, under these conditions, the Sn−O bond in the $(n\text{-Bu}_3Sn)_2O$ product

dx.doi.org/10.1021/ja409559h | J. Am. Chem. Soc. 2013, 135, 19304−19310

is formed mostly via oxygen transfer from the polyoxometalate. The computational and ^{18}O labeling studies with $^{18}O_2$ indicate that following the oxygen transfer a reduced complex with an intact Keggin structure, $H_7PV^{IV}{}_2Mo_{10}O_{40}$, is formed by reaction with water and then oxidized with O_2. On the other hand, the same experiments and those with S_8 show that the source of oxygen in 1-butanol is at least mostly from O_2. The mode of reaction of O_2 with the reduced polyoxometalate−substrate intermediate species $R{-}H_5PV^{IV}V^{V}Mo_{10}O_{40}$ remains an important topic to be studied by experiment and computation, and both inner-sphere and outer-sphere reactions should be considered.[26,27] Another comment to make is that cleavage of the initially formed n-$Bu_4Sn^{\bullet+}$ could also form butyl radicals, as suggested in *stoichiometric* oxidations with Ir(IV) and Fe(III),[13a] which could be trapped by O_2 to yield an intermediate peroxo species that should yield equimolar amounts of 1-butanol and n-butanal.[13a] The absence of an aldehyde product and the absence of oxygenates from the more stable secondary carbon radical, as well as the known inhibition of free radical reactions by $H_5PV_2Mo_{10}O_{40}$,[27] all argue against such a reaction pathway. In a more general context, the insertion of an oxygen atom from O_2 into a metal−carbon bond is an important step in the development of a catalytic oxidation of alkanes to alcohols through a combination of C−H bond activation and oxygen atom insertion.

EXPERIMENTAL SECTION

Oxidation Reactions. Reactions under anaerobic conditions were carried out in 15 mL Ace glass pressure tubes. The tubes were charged with the appropriate amounts of substrate, catalyst, and solvent and were gently flushed with argon for 5 min. The tubes were then frozen with liquid N_2, pumped down, filled with argon, and then thawed. This procedure was repeated three times until final pressurization to 2 bar of argon. Thus, in a typical anaerobic experiment, $H_5PV_2Mo_{10}O_{40}\cdot 34H_2O$ (23 mg, 10 μmol) was dissolved in acetonitrile (1 mL), and then n-Bu_4Sn (10 μL, 29 μmol) was placed in a 15 mL Ace glass pressure tube. The resulting solution was taken through several gas/degas cycles as noted above. The glass tube was placed in an oil bath at 70 °C. After 2 h the solution turned dark green. The reaction mixture was cooled, and the solution was analyzed for n-Bu_4Sn conversion and product formation by GC and GC-MS. GC and GC-MS analyses were preformed on aliquots directly withdrawn from the reaction mixture after dilution with dichloromethane and addition of n-decane as an external standard.

Insertion of ^{18}O into products from $H_5PV_2Mo_{10}{}^{18}O_{40}$ (40−50% ^{18}O) was measured by reacting n-Bu_4Sn and $H_5PV_2Mo_{10}{}^{18}O_{40}$ (10 mM) in acetonitrile at 70 °C. ^{18}O incorporation was calculated from the mass spectra by comparing peak intensities. For 1-butanol peaks at m/z 73 and 75 were compared. ^{18}O incorporation for $(Bu_3Sn)_2O$ was determined by ESI-MS by comparing peak intensities at m/z 597 and 599, respectively. Kinetic profiles of the interaction of n-Bu_4Sn with $H_5PV_2Mo_{10}O_{40}$ were obtained by purging a solution of 2 μmol of $H_5PV_2Mo_{10}O_{40}$ in 2 mL of acetonitrile with argon for 20 min in a quartz cuvette and then heating to 50 °C. The reaction was initiated by the addition of 29 μmol of n-Bu_4Sn. The reaction was followed by reduction of the polyoxometalate at λ_{max} 750 nm. Pseudo-first-order rate constants (r^2 = 0.99) were computed from the absorption data.

Computational Methods. All computations were done using a locally modified version of the Gaussian 09 package. Geometry optimizations and harmonic frequency evaluations have been performed using the nonempirical GGA density functional[28] PBE[29] in conjunction with the PC1 basis set. The latter is a combination of Jensen's polarization consistent pc-1 basis set[30] for the main-group elements with the Stuttgart−Dresden−Dolg (SDD) basis set−RECP (relativistic energy-consistent pseudopotential) combination[31] for molybdenum and vanadium. To the latter wa added a single f-type polarization function, the exponent being the geometric average of the two f exponents given by Martin and Sundermann.[32] This combination is of double-ζ plus polarization quality. The cc-pVDZ-PP basis set−RECP combination was used for tin.[33] As this is well-known to speed up "pure" DFT calculations on large systems by 1−2 orders of magnitude, we applied the density fitting (DF) approximation[34] for calculating the two-electron (Coulomb) integrals. The automatic algorithm as implemented in Gaussian 09 generated the auxiliary basis sets required for this. Thus, the geometries of all the complexes were optimized at the PBE-DF/PC1 level of theory without symmetry constraints. Subsequently, single-point calculations at the optimized geometries were performed using the empirical hybrid meta-GGA functional M06[35] combined with the same basis set (M06/PC1), as well as using the PBE functional but combined with a larger AUG-PC1 basis set. The AUG-PC1 basis set represents a combination of the aug-pc-1 basis set on the main-group elements,[36] the aug-cc-pVDZ-PP basis set on tin,[31] and SDD basis set with added f basis functions on molybdenum and vanadium. The final level of theory applied in the present work is thus an additive approximation: E_e[M06/AUG-PC1] ≈ E[PBE-DF/AUG-PC1] − E[PBE-DF/PC1] + E[M06/PC1]. Bulk solvent effects of the acetonitrile medium have been calculated at the M06/PC1 level via the self-consistent reaction field (SCRF) method,[37] using the continuum solvation model COSMO as it is implemented in Gaussian 09.[38] Dispersion interactions within the computed structures were approximately taken into account by adding the D2 empirical dispersion correction term,[39] with an s_6 value of 0.25, as suggested by Karton et al. for the M06 functional.[40] For qualitative interpretation of the computational results, the M06/PC1 electron density of the structures in optimized geometries was analyzed using natural bond orbital (NBO) analysis.[41]

The performance of the applied computational method in the prediction of optimized geometries and in energies of protonated polyoxometalates in the absence and in the presence of additional coordinated species was discussed in our previous papers.[16] The ability of the computational method to accurately predict relative energies of species with different multiplicity states, usually not a trivial task for DFT methods, is especially important for the present study. Using small molybdenum and vanadium oxide model complexes, relative to basis set limit CCSD(T) benchmark data, we found RMSDs of 3.49 and 7.26 kcal/mol, respectively, for electron transfer (ET) and coupled proton and electron transfer (CPET) reactions. This is close to the performance of an accurate double-hybrid method such as B2GP-PLYP. These latter results will be discussed in detail in a forthcoming full paper.

ASSOCIATED CONTENT

Supporting Information

Text, tables, and figures giving additional experimental information and data and details of the calculations. This material is available free of charge via the Internet at http://pubs.acs.org.

AUTHOR INFORMATION

Corresponding Author

Ronny.Neumann@weizmann.ac.il

Notes

The authors declare no competing financial interest.

ACKNOWLEDGMENTS

This research was supported by the Israel Science Foundation Grant No. 1073/10 and the Helen and Martin Kimmel Center for Molecular Design. Dr. Lev Weiner is thanked for the EPR measurements. J.M.L.M. holds the Baroness Thatcher Professorial Chair of Chemistry. R.N. is the Rebecca and Israel Sieff Professor of Chemistry.

REFERENCES

(1) (a) Sheldon, R. A.; Kochi, J. K. *Metal-catalyzed oxidations of organic compounds*; Academic Press: New York, 1981. (b) Hermans, I.; Peeters, J.; Jacobs, P. A. *Top. Catal.* **2008**, *48*, 41−48.

(2) (a) Tinberg, C. E.; Lippard, S. J. *Acc. Chem. Res.* **2011**, *44*, 280−288. (b) Friedle, S.; Reisner, E.; Lippard, S. J. *Chem. Soc. Rev.* **2010**, *39*, 2768−2779. (c) Rosenzweig, A. C. *Biochem. Soc. Trans.* **2008**, *36*, 1134−1137. (d) Guengerich, F. P. *Arch. Biochem. Biophys.* **2011**, *507*, 255.

(3) (a) Shilov, A. E.; Shulpin, G. B. *Russ. Chem. Rev.* **1987**, *56*, 442−464. (b) Labinger, J. A.; Bercaw, J. E. *Nature* **2002**, *417*, 507−514. (c) Periana, R. A.; Taube, D. J.; Gamble, S.; Taube, H.; Satoh, T.; Fujii, H. *Science* **1998**, *280*, 560−564. (d) Muehlhoefer, M.; Strassner, T.; Herrmann, W. A. *Angew. Chem., Int. Ed.* **2002**, *41*, 1745−1747. (e) Lin, M.; Shen, C.; Garcia-Zaya, E. A.; Sen, A. *J. Am. Chem. Soc.* **2001**, *123*, 1000−1001. (f) Periana, R. A.; Mironov, O.; Taube, D.; Bhalla, G.; Jones, C. J. *Science* **2003**, *301*, 814−818.

(4) (a) Lin, M.; Hogan, T.; Sen, A. *J. Am. Chem. Soc.* **1997**, *119*, 6048−6053. (b) Bar-Nahum, I.; Khenkin, A. M.; Neumann, R. *J. Am. Chem. Soc.* **2004**, *126*, 10236−10237.

(5) Pouy, M. J.; Milczek, E. M.; Figg, T. M.; Otten, B. M.; Prince, B. M.; Gunnoe, T. B.; Cundari, T. R.; Groves, J. T. *J. Am. Chem. Soc.* **2012**, *134*, 12920−12923.

(6) (a) Brown, S. N.; Mayer, J. M. *J. Am. Chem. Soc.* **1996**, *118*, 12119−12133. (b) Alsters, P. L.; Boersma, J.; van Koten, G. *Organometallics* **1993**, *12*, 1629−1635. (c) Alsters, P. L.; Teunissen, H. T.; Boersma, J.; Spek, A. L.; van Koten, G. *Organometallics* **1993**, *12*, 4691−4696. (d) Matsunaga, P. T.; Hillhouse, G. L.; Rheingold, A. L. *J. Am. Chem. Soc.* **1993**, *115*, 2075−2077. (e) Koo, K.; Hillhouse, G. L.; Rheingold, A. L. *Organometallics* **1995**, *14*, 456−460.

(7) (a) Conley, B. L.; Ganesh, S. K.; Gonzales, J. M.; Tenn, W. J., III; Young, K. J. H.; Oxgaard, J.; Goddard, W. A., III; Periana, R. A. *J. Am. Chem. Soc.* **2006**, *128*, 9018−9019. (b) Gonzales, J. M.; Distasio, R., Jr.; Periana, R. A.; Goddard, W. A., III; Oxgaard, J. *J. Am. Chem. Soc.* **2007**, *129*, 15794. (c) Bischof, S. M.; Cheng, M.-J.; Nielsen, R. J.; Gunnoe, T. B.; Goddard, W. A., III; Periana, R. A. *Organometallics* **2011**, *30*, 2079−2082.

(8) (a) Khenkin, A. M.; Neumann, R. *Angew. Chem., Int. Ed.* **2000**, *39*, 4088−4090. (b) Khenkin, A. M.; Weiner, L.; Wang, Y.; Neumann, R. *J. Am. Chem. Soc.* **2001**, *123*, 8531−8542.

(9) Khenkin, A. M.; Neumann, R. *J. Am. Chem. Soc.* **2008**, *130*, 11876−11877.

(10) (a) Neumann, R. *Inorg. Chem.* **2010**, *49*, 3594−3601. (b) Neumann, R.; Khenkin, A. M. *Chem. Commun.* **2006**, 2529−2538.

(11) Altenau, J. J.; Pope, M. T.; Prados, R. A.; So, H. *Inorg. Chem.* **1975**, *14*, 417−421.

(12) (a) Goldberg, H.; Kaminker, I.; Goldfarb, D.; Neumann, R. *Inorg. Chem.* **2009**, *48*, 7947−7952. (b) Kaminker, I.; Goldberg, H.; Neumann, R.; Goldfarb, D. *Chem. Eur. J.* **2010**, *16*, 10014−10020.

(13) (a) Wong, C. L.; Kochi, J. K. *J. Am. Chem. Soc.* **1979**, *101*, 5593−5603. See also research on oxidation of tin hydrides and formation of tin benzoates: (b) Wong, C. L.; Klinger, R. J.; Kochi, J. K. *Inorg. Chem.* **1980**, *19*, 423−430. (c) Xu, H. L.; Yin, H. D.; Gao, Z. J.; Li, G. *J. Organomet. Chem.* **2006**, *691*, 3331−3335.

(14) 1-Butanol: ^{13}C NMR δ 62.5, 34.9, 19.3, 13.9 ppm; ^{1}H NMR δ 3.65 (t, 2H), 1.32 (m, 2H), 0.94 (m, 2H), 0.85 (t, 3H) ppm. (n-$Bu_3Sn)_2O$: ^{13}C NMR 29.8, 28.1, 19.3, 13.7 ppm; ^{1}H NMR δ 1.65 (m, 2H), 1.37 (m, 4H), 0.95 (t, 3H) ppm.

(15) $H_4PVMo_{11}O_{40}$ was used because it is less susceptible to fragmentation under ESI conditions in comparison to $H_5PV_2Mo_{10}O_{40}$ yet has similar reactivity (Table S1, Supporting Information).

(16) (a) Efremenko, I.; Neumann, R. *J. Am. Chem. Soc.* **2012**, *134*, 20669−20680. (b) Efremenko, I.; Neumann, R. *J. Phys. Chem. A* **2011**, *115*, 4811−4826.

(17) $H_5PV_2Mo_{10}O_{40}$ is a mixture of five isomers that are inseparable. The 1,2-$H_5PV_2Mo_{10}O_{40}$ isomer is known to be active in oxygen transfer.[10a,11]

(18) A reviewer noted that, given a measured $\Delta G^{\ddagger}_{323}$ = 23.6 kcal/mol, the ΔG_{343} value for CPET of 16.1 kcal/mol does not rule out that mechanism. However, the most energetically favorable CPET is by hydrogen atom transfer (HAT) at the β carbon atom to form $Bu_3SnCH_2CHC_2H_5^{\bullet}$, which decomposes to linear butenes and $Bu_3Sn^{\bullet}$. HAT at the α or γ carbon atoms are 7.3 and 6.4 kcal/mol less favorable, respectively. No reasonable route to the selective formation of 1-butanol as the only alcohol by CPET was found.

(19) A relaxed scan of the singlet potential energy surface (PES) of n-Bu_4Sn shows that the distortion of ∠C−Sn−C from 109.7 to 166.8° yields an increase in energy of 21.0 kcal/mol.

(20) The Wiberg bond index W_{AB} for the atom pair A, B is defined as $\sum_{ij}P_{ij}^2$: i.e., the sum of squares of all density matrix elements $\sum_{ij}P_{ij}$ where basis functions i and j are located on atoms A and B, respectively. Wiberg, K. B. *Tetrahedron* **1968**, *24*, 1083−1096. For the theoretical background of bond order indices, see: Mayer, I. *J. Comput. Chem.* **2007**, *28*, 204−221.

(21) The APT charge on the O atom bound to $SnBu_3^+$ in the defect complex [$SnBu_3^+$-(**3**-H_2O)] is −1.23, in comparison to APT charges in the range of −0.57 to −0.85 on other bridging oxygen atoms in **3**.

(22) The calculations were only on one isomer of the polyoxometalate; others may react somewhat differently.[10,11] The possibility of two ET reactions on the same polyoxometalate molecule is also a possibility that was not investigated.

(23) A previous report on the anaerobic oxidation of tetraalkyltin compounds with iridium(IV) or iron(III) complexes[12a] also suggests that the initially formed $R_4Sn^{\bullet+}$ is cleaved but yielded $R_3Sn^+X^-$ and RX, where X is an anion such as Cl^- or ClO_4^-.

(24) Hirao, H.; Kumar, D.; Chen, H.; Neumann, R.; Shaik, S. *J. Phys. Chem. C* **2007**, *111*, 7711−7719.

(25) Gao, S.; Moffat, J. B. *Catal. Lett.* **1996**, *42*, 105−111.

(26) Snir, O.; Wang, Y.; Tuckerman, M. E.; Geletii, Y. V.; Weinstock, I. A. *J. Am. Chem. Soc.* **2010**, *132*, 11678−11691.

(27) Neumann, R.; Levin, M. *J. Am. Chem. Soc.* **1992**, *114*, 7278−7286.

(28) (a) Kohn, W.; Sham, L. J. *Phys. Rev. A* **1965**, *140*, 1133−1138. (b) Parr, R. G.; Yang, W. *Density Functional Theory of Atoms and Molecules*; Oxford University Press: New York, 1970; p 230.

(29) Perdew, J. P.; Burke, K.; Ernzerhof, M. *Phys. Rev. Lett.* **1996**, *77*, 3865−3868.

(30) (a) Jensen, F. *J. Chem. Phys.* **2001**, *115*, 9113−9125. (b) Jensen, F. *J. Chem. Phys.* **2002**, *116*, 7372−7379.

(31) Dolg, M. In *Modern Methods and Algorithms of Quantum Chemistry*; Grotendorst, J., Ed.; NIC: Jülich, Germany, 2000; Vol. *1*, pp 479−508.

(32) Martin, J. M. L.; Sundermann, A. *J. Chem. Phys.* **2001**, *114*, 3408−3420.

(33) Peterson, K. A.; Figgen, D.; Goll, E.; Stoll, H.; Dolg, M. *J. Chem. Phys.* **2003**, *119*, 11113−11123.

(34) (a) Dunlap, B. I. *J. Chem. Phys.* **1983**, *78*, 3140−3142. (b) Dunlap, B. I. *J. Mol. Struct. (THEOCHEM)* **2000**, *529*, 37−40. (c) Nadykto, A. B.; Dua, H.; Yu, F. *Vib. Spectrosc.* **2007**, *44*, 286−296.

(35) Zhao, Y.; Truhlar, D. G. *J. Chem. Phys.* **2006**, *125*, 194101.

(36) (a) Jensen, F. *J. Chem. Phys.* **2002**, *117*, 9234−9240. (b) Jensen, F. *J. Chem. Phys.* **2003**, *118*, 2459−2463.

(37) Cossi, M.; Scalmani, G.; Rega, N.; Barone, V. *J. Chem. Phys.* **2002**, *117*, 43−54.

(38) (a) Klamt, A.; Schürmann, G. *J. Chem. Soc., Perkin Trans. 2* **1993**, 799−805. (b) Barone, V.; Cossi, M. *J. Phys. Chem. A* **1998**, *112*, 1995−2001.

(39) (a) Grimme, S. *J. Comput. Chem.* **2006**, *27*, 1787−1799. See also: (b) Schwabe, T.; Grimme, S. *Phys. Chem. Chem. Phys.* **2007**, *9*, 3397−3406. (c) Schwabe, T.; Grimme, S. *Acc. Chem. Res.* **2008**, *41*, 569−579.

(40) Karton, A.; Tarnopolsky, A.; Lamère, J.-F.; Schatz, G. C.; Martin, J. M. L. *J. Phys. Chem. A* **2008**, *112*, 12868−12886.

(41) Reed, A. E.; Curtiss, L. A.; Weinhold, F. *Chem. Rev.* **1988**, *88*, 899−926.